

Articles All fields Author
Images Journal/Book title Volume Issue Page



 **IDC Manufacturing Insights Whitepaper:**
Designing Environmental Sustainability into Product Research and Development

[Thumbnails](#) | [Full-Size images](#)

[▶ View](#)

[▶ View](#)

- 2. Formulation of the problem and finite element modeling
- 3. Result
- 4. Conclusion

References

1. Introduction

With the development of society, people have more and more demands for automobile passive safety and fuel economy, which requires the improvement of automobile structure crashworthiness and lightweighting degree [1] and [2]. Besides, in the case of passenger transportation systems, it is also necessary to ensure that the passengers can tolerate an impact. In other words, the magnitude of the peak in the crushing force–axial displacement characteristics which determine the deceleration amount and the value of Head Injury Criterion must be tolerable to the passenger.

The automobile body crashworthiness and lightweighting can be achieved by structure modification or material replacement. Latest studies have shown material replacement is generally more effective in automobile crashworthiness and lightweighting than structure modification [3].

In this task material replacement using different types of joining in S-frame and their effects on crashworthiness, the magnitude of the peak in the crushing force–axial displacement characteristics and lightweighting of S-frame are studied.

Design, calculation and testing of lightweight and energy absorbing front rails of passenger cars have been the subject of extensive studies over the past two decades. Ohkami et al. [4] and Abe et al. [5] carried out experimental and numerical studies on the collapse behaviors of S-shaped beams. They investigated the deformation modes and the force–displacement relations.

Kim and Wierzbicki [6] addressed the design aspect of a front side rail structure of an automobile body, which is a steel spot-welded sheet metal S-frame, from the point of view of weight efficiency and energy absorption. They investigated various methods of internal strengthening, in order to improve structural crashworthiness and performance.

In order to reduce the automobile weight, aluminum and magnesium alloys, high-strength steel, composite material, and so on, are widely used as crashworthiness and lightweighting materials to replace the traditional material of mild steel [3].

Among these materials, aluminum is examined in this paper in a hybrid S-frame which is constructed from two parts. One part is made of mild steel which has higher stiffness and better characteristic against bending and the other part is made of aluminum which has better energy absorption characteristic and lower weight. Through comparison with a simple S-frame made of mild steel advantages of such a hybrid S-frame is shown.

2. Formulation of the problem and finite element modeling

The first structure which is considered in this study is a thin-walled S-shaped frame with a hat-type cross-section. The S-frame is an assembly of two main sheet metal parts. Spot-welding is used to join the components. This model is named as the base model through this paper. The model can represent a highly idealized front side rail of a car. The reference cross-section without side flange is square with the aspect ratio (b/t) equal to 50 ($80/1.6=50$), where b is the web width and t is the thickness. The width of side flange is 30 mm. The S-shaped frame is composed of two circular arches in both the Z and Y plane. The detailed dimensions are given in Fig. 1.

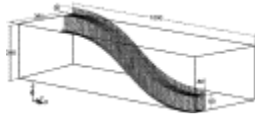
- Hardi
Ency
- 2.06
Com
- 2.03
Com
- More

View F



CrossB
leading

Discov
pollinat



[Full-size image \(10K\)](#)

Fig. 1.

Configuration of the S-frame model (all dimension are in mm).

One end of the model is fully clamped, and the load is applied on the other end as the velocity boundary condition in the X -direction. All the degrees of freedom except for X translation are fixed on the moving end to model the actual deformation of the front side rail of a car under frontal collision. Because the geometry of the model is S-shaped, the member will be subjected to a combination of axial compression, bending, and tensional moment. Therefore, from the point of view of loading, the above model corresponds well to a real front rail of a passenger car (Fig. 2).

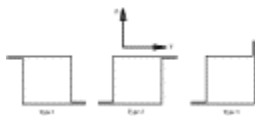


[Full-size image \(15K\)](#)

Fig. 2.

Loading condition.

Various orientations and cross-sectional shapes which are investigated in this study are shown in Fig. 3.



[Full-size image \(3K\)](#)

Fig. 3.

Various cross-section shapes considered.

For the numerical simulation of a typical collapse of S-frame using FE Code LS-DYNA, the following calculation steps are conducted:

- (1) The shell is modeled using 4-node 'shell' elements with three integration points through thickness (Belytschko–Tsai 'shell' element), which present macroscopic mesh distortion in a better way. The numbers of elements used to model the S-frame geometry are 8288 shell elements and are shown in Fig. 4.



Fig. 4.

Finite element model.

- (2) The S-frame material is steel with mechanical properties of Young's modulus $E = 2.07E5$ N/mm², initial yield stress $\sigma_y = 335.47$ N/mm², and Poisson's ratio $\nu = 0.3$. The detailed stress–strain relation for this material is shown in Fig. 5. In the spot welds material is treated in a same manner, considering an initial yield point of 550 N/mm². The welding pitch is considered 30 mm. In any case, the material was modeled as an isotropic elastic–plastic material, characterized by elastoplastic behavior with strain hardening.

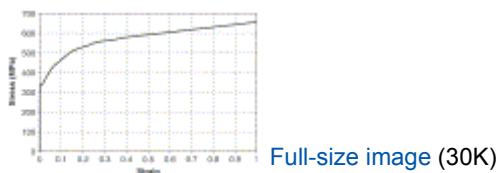


Fig. 5.

Stress–strain curve of the steel used in this study.

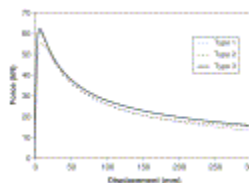
- (3) The nodes in the moving end are connected with a rigid body. This configuration can be interpreted as a virtual rigid massless plate attached to the moving end of the beam. The load in the form of ramped velocity boundary condition is applied at the center of gravity of this rigid body. The ramping time is 0.05 s, and a constant velocity is 2000 mm/s. For the moving end of S-frame only one degree of freedom is considered, corresponding to the movement of the rigid plate.
- (4) The single surface type of interface is selected to simulate the situation during crushing, when elements of the S-rail contact each other creating a new interface. This contact definition requires thickness to be taken into account for a shell that is modeled by using shell elements. The single surface contact type uses nodal normal projections and, therefore, it prevents the elements from penetrating the plate surface during crushing. It also permits relative motion considering Coulomb friction coefficients equal to 0.3 and 0.2 for the static and dynamic conditions, respectively.

The second and the third structures which are used in this task are shown in Fig. 10. These structures represent a two materials (aluminum and steel) S-frame with different types of connection for two segments of S-frame. These structured are named as Model 1 and Model 2 throughout this paper.

3. Result

In order to investigate crashworthiness, lightening and the magnitude of the peak in the crushing force–axial displacement characteristics, three models of S-frame are studied in this task.

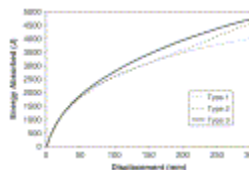
In the first step of calculations, using base model (Fig. 1) three types of cross-sections shown in Fig. 3 are analyzed. The evaluation of sectional force response energy absorption and the deformed shapes of the model are shown in Fig. 6, Fig. 7 and Fig. 8. The force response is taken from the clamped end, and the computer run is made up to deformation of 30% of the initial length. In all models the force increases up to the peak value, decays dramatically, and then stays constant around 15–20 kN. The trends of these results have a good agreement with the result which is obtained by Kim and Wierzbicki [5]. Global bending collapse is dominating the response, and a single local axial fold is observed near the clamped end or moving end. The original square hat-type cross-section is entirely flattened out over the central part of the member in all models, see Fig. 8. The bending resistance of the flattened out section is very low, which explains a small magnitude of the force response.



[Full-size image \(22K\)](#)

Fig. 6.

Force response of Type 1–3.



[Full-size image \(24K\)](#)

Fig. 7.

Energy absorbed by various cross-sections (refer to Fig. 3).



[Full-size image \(28K\)](#)

Fig. 8.

Deformed shapes of the various models.

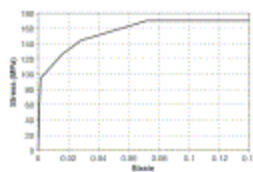
Table 1 shows the comparison of maximum energy absorption for Types 1–3. Among these three types of cross-section considered in this study type 3 shows a higher energy absorption and force response. Therefore, this type of cross-section is chosen for hybrid S-frame.

Table 1. Comparison of maximum energy absorption for Types 1–3

	Weight (kg)	Wall thickness (mm)	Maximum energy absorption (J)
Type 1	5.794	1.6	4014.09
Type 2	5.794	1.6	4586.74
Type 3	5.794	1.6	4738.48

[Full-size table](#)

In order to improve the energy absorption and lightening characteristic and study the maximum amount of crushing force, two hybrids S-frame containing steel and aluminum parts with different kinds of connection for two parts are considered and shown in **Fig. 10** (Models 1 and 4442). As seen from **Fig. 10** nearly 33% of hybrid S-frame is made of aluminum with mechanical properties which are shown in **Fig. 9**. This figure (33%) is found through optimization of energy absorption of hybrid S-frame which contain steel and aluminum segment with the same wall thickness.



[Full-size image \(30K\)](#)

Fig. 9.

Stress–strain curve of the aluminum used in this study.



[Full-size image \(48K\)](#)

Fig. 10.

Various connection types considered.

Fig. 11 and **Fig. 12** show FEM models of hybrid S-frame. For the numerical simulation of hybrids S-frame collapse using FE Code LS-DYNA the same assumptions like base model are used.



[Full-size image \(17K\)](#)

Fig. 11.

Finite element model of hybrid S-frame (Model #1).

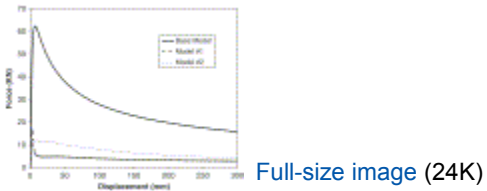


[Full-size image \(14K\)](#)

Fig. 12.

Finite element model of hybrid S-frame (Model #2).

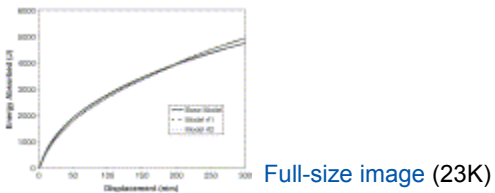
Effects of different types of connection on force response and energy absorption of S-frame are shown in Fig. 13 and Fig. 14. In these figures all three considered S-frames are made of steel and the wall thickness in all models is 1.6 mm. As it is seen the peak of the force in base model is many times higher than Models 1 and 2. However the energy absorbed by various model is nearly the same. On the other hand Models 1 and 2 have better force response and cause less injury for the passengers.



[Full-size image \(24K\)](#)

Fig. 13.

Effects of connection type on force response.

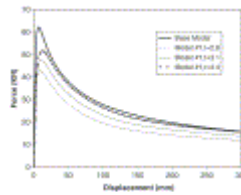


[Full-size image \(23K\)](#)

Fig. 14.

Effect of connection type on energy absorption by S-frame.

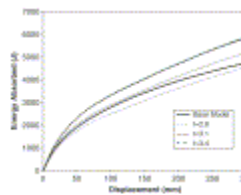
In Fig. 15 and Fig. 16 Model 1 is studied considering various wall thickness for aluminum segment. In these figures the wall thickness of steel part is 1.6 mm and the thickness of aluminum part varies from 2.8 to 3.4. As it is seen the picks of the force response and the amounts of energy absorbed are increased with increasing the thickness of the aluminum part.



[Full-size image \(29K\)](#)

Fig. 15.

Force response of S-frame (Model # 1) for various thickness of aluminum part.

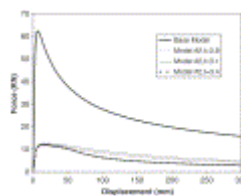


[Full-size image \(28K\)](#)

Fig. 16.

Energy absorbed by S-frame (Model # 1) for various thicknesses of aluminum part.

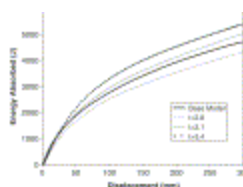
In Fig. 17 and Fig. 18 Model 2 is studied considering various wall thickness for aluminum segment. In these figures the wall thickness of steel part is 1.6 mm and the thickness of aluminum part varies from 2.8 to 3.4. As it is seen the picks of the force response are nearly the same for all three thicknesses of aluminum and many times lesser than base model and Model 1, while the amounts of energy absorbed are increased with increasing the wall thickness of the aluminum part and are higher than base model for aluminum thickness more than 3.1 mm.



[Full-size image \(27K\)](#)

Fig. 17.

Force response of S-frame (Model # 2) for various thicknesses of aluminum part.



Full-size image (29K)

Fig. 18.

Energy absorbed by S-frame (Model #2) for various thicknesses of aluminum part.

Fig. 19 shows deformed shapes of different models with various thicknesses. Global bending collapse is dominating the response, and a single local axial fold is observed near the clamped end or moving end. The original square hat-type cross-section is entirely flattened out over the central part, in Model 1 before connection and in Model 2 just at connection area; see Fig. 19. The bending resistance of the flattened out section is very low, which explains a small magnitude of the force response.



Full-size image (92K)

Fig. 19.

Deformed shapes of various models with various thicknesses.

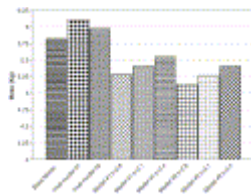
Table 2 and Fig. 20 and Fig. 21 are the comparison of mass, maximum energy absorbed and the peak of force response for various models. As it is seen from these figures using hybrid S-frame with the connection type used in Model 2 can decrease the peak of force and total weight and increase the energy absorbed comparing to base model.

Table 2. Comparison of mass and maximum energy absorbed for various models

	Material	Thickness (mm)	Weight (kg)	Maximum energy absorbed (J)	Crashworthiness change (%)
Base model	Steel	1.6	5.794	4726.28	0
1Mat,model #1	Steel	1.6	6.085	4917.44	+4
1Mat,model #2	Steel	1.6	5.948	4752.03	+0.5
Model #1	Steel	1.6	5.262	4550.65	-3.7
	Aluminum	2.8			
Model #1	Steel	1.6	5.395	5187.67	+9.8
	Aluminum	3.1			
Model #1	Steel	1.6	5.528	5845.96	+23.7

	Material	Thickness (mm)	Weight (kg)	Maximum energy absorbed (J)	Crashworthiness change (%)
	Aluminum	3.4			
Model #2	Steel	1.6	5.119	4348.18	-8
	Aluminum	2.8			
Model #2	Steel	2.8	5.253	5043.74	+6.7
	Aluminum	3.1			
Model #2	Steel	1.6	5.387	5416.04	+14.6
	Aluminum	3.4			

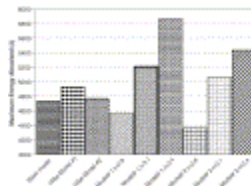
[Full-size table](#)



[Full-size image \(107K\)](#)

Fig. 20.

Comparison of total mass between various models.



[Full-size image \(96K\)](#)







Fig. 21.

Comparison of maximum energy absorbed between various models.

4. Conclusion

Numerical calculation such as those in [4] and [5] enable engineer to assess whether a structure design is capable of withstanding the forces generated during an impact and absorbing the impact energy without excessive damage. However in the case of passenger transportation systems, it is also necessary to ensure that the passengers can tolerate an impact. The magnitude of the peak in the crushing force–axial displacement characteristics is sometimes much larger than the mean force associated with subsequent crushing force–axial displacement characteristics as is shown in Fig. 13. However, as it is shown in this task, it is possible to manufacture a hybrid S-frame to eliminate this initial peak, which is undesirable because of the large associated decelerations during an impact event and, to improve energy absorption and lightweighting specifications.

References

- [1] E. Schubert, M. Klassen, I. Zemer, C. Walz and G. Sepold, Light weight structures produced by laser beam joining for future applications in automobile and aerospace industry. *J Mater Process Technol*, **115** (2001), pp. 2–8. 
- [2] K. Yamane and S. Furuhashi, A study on the effect of the total weight of fuel and fuel tank on the driving performances of cars. *Int J Hydrogen Energy*, **23** (1998), pp. 825–831. 
- [3] Y. Li, Z. Lin, A. Jiang and G. Chen, Use of high strength steel sheet for lightweight and crashworthy car body. *Mater Design*, **24** (2003), pp. 177–182. 
- [4] Ohkami Y, et al. Collapse of thin-walled curved beam with closed-hat section—Part 1: study on collapse characteristics. SAE Paper 900460, 1990.. 
- [5] Abe K, et al. Collapse of thin-walled curved beam with closed-hat section—Part 2: simulation by plane plastic hinge model. SAE Paper 900461, 1990.. 
- [6] H-S. Kim and T. Wierzbicki, Effect of the cross-sectional shape of hat-type cross-sections on crash resistance of an “S”-frame. *Thin-Walled Struct*, **39** (2001), pp. 535–554. 



Corresponding author

Copyright © 2006 Elsevier Ltd. All rights reserved.

Thin-Walled Structures

Volume 44, Issue 4, April 2006, Pages 407-414

Home Browse Search My settings My alerts Shopping cart

About ScienceDirect
[What is ScienceDirect](#)
[Content details](#)
[Set up](#)
[How to use](#)
[Subscriptions](#)
[Developers](#)

Contact and Support
[Contact and Support](#)

About Elsevier
[About Elsevier](#)
[About SciVerse](#)
[About SciVal](#)
[Terms and Conditions](#)
[Privacy policy](#)
[Information for advertisers](#)

Copyright © 2011 Elsevier B.V. All rights reserved. SciVerse® is a registered trademark of Elsevier Properties S.A., used under license Elsevier B.V.